ChemComm

FEATURE ARTICLE

Cite this: *Chem. Commun.*, 2018, **54**, 1934

Scanning electrochemical microscopy at the nanometer level

Tianhan Kai, Cynthia G. Zoski and Allen J. Bard *

Received 21st December 2017,
Accepted 24th January 2018

DOI: 10.1039/c7cc09777h

rsc.li/chemcomm

This review describes how one can perform nanometer (nm)-scale SECM experiments through advances in tip fabrication and positioning and instrumentation design. Basic SECM methodology including instrumentation and feedback and generation/collection modes are discussed. Aspects of nanoscale SECM including fabrication of nm-sized electrodes and nano SECM instrumentation are also described. State of the art applications related to nanogaps (*i.e.*, rapid homogeneous reactions and short-lived intermediates; heterogeneous electron transfer kinetics; nanoparticles (NPs) and clusters) and nanoscale imaging (*e.g.*, single NPs, single biological samples, combined methods) are described. Future possibilities and prospects are suggested that might lead to even better resolution, thus introducing SECM electrochemical imaging to the single atom level.

1. Introduction

When scanning electrochemical microscopy (SECM) was introduced in 1989,[1] ultramicroelectrode (UME) size was limited to the μm scale. Thus, although it introduced the concept of "chemical imaging" and determination of absolute tip distance, it did not have the imaging resolution of other scanning probe methods like STM and AFM.[2] However in the intervening years, as described below, through the efforts of many groups, much smaller UMEs became available and instrumentation for moving tips was improved. The attendant SECM resolution improved by at least two orders of magnitude.[3–6]

This review discusses these developments and describes how one can perform nanometer (nm)-scale SECM experiments. It describes state of the art applications of the technique and suggests possible advances that might lead to even better resolution, thus introducing this alternative approach to "imaging" to the single atom level and rivaling electron microscopic and scanning probe methods.

Center for Electrochemistry, Department of Chemistry, The University of Texas at Austin, Austin, TX, 78712, USA. E-mail: ajbard@cm.utexas.edu

Tianhan Kai

Tianhan Kai received his PhD at Central South University, China in analytical chemistry in 2015 under the supervision of Prof. Feimeng Zhou. Presently he is a postdoctoral fellow with Prof. Allen J. Bard at the University of Texas at Austin (UT Austin). His research interests include applications of nanoscale SECM, coupled analytical techniques and chemical instrumentation and development of high-throughput biosensors for disease diagnosis.

Cynthia G. Zoski

Cynthia G. Zoski is the Associate Director for the Center of Electrochemistry and a Research Professor in the Department of Chemistry at the University of Texas at Austin. Her research interests include electroanalytical chemistry involving ultramicroelectrodes (UMEs), nanoelectrodes, scanning electrochemical microscopy (SECM), and electrocatalysis. Dr Zoski is the coauthor of Electrochemical Methods, 2nd edition: Instructor's Solution Manual (Wiley, 2001) and Student's Solution Manual (Wiley 2002), editor of the Handbook of Electrochemistry (Elsevier, 2007), co-editor of Electroanalytical Chemistry (Taylor and Francis), and author or co-author of over 70 papers and book chapters.

2. SECM basics

SECM provides both chemical and topographic information, especially about surfaces immersed in a solution.[2] For example, our group and others have used SECM to investigate redox properties of surfaces or adsorbates, in studying highly localized chemical reactions, and to induce redox reactions at liquid/liquid and liquid/solid interfaces. SECM is based on moving a small (*i.e.*, micrometer (μm) to nm-sized UME) tip electrode of various geometries (*e.g.*, disk, ring, sphere) very close to a substrate surface (*i.e.*, in the z direction for probing surfaces, in the x–y directions for surface imaging).

2.1 SECM instrumentation

A typical SECM instrument (Fig. 1) is composed of a four-electrode electrochemical cell, a three dimensional (*e.g.*, x, y, z) positioning system containing piezo positioners for precise movement of the tip (and, a system, *e.g.* a stepper motor, for coarse positioning), a bipotentiostat for control of the current and potential at both the UME tip and the substrate, and a data acquisition and analysis system controlled by a computer.[7] For specialized applications involving biological sample imaging, for example, additional components (*e.g.*, an inverted microscope, a distance control system) may be added.

2.2 SECM modes

Since the 1990s, a number of modes of SECM that have later been applied to nm-scale measurements have been developed for various applications, including the feedback, generation/collection (G/C), shielding (or redox competition), and potentiometric modes.[2] Principles of these modes can be found in a number of publications and reviews.[7–16] Among them, the feedback mode and generation/collection (G/C) modes were the first to be introduced and widely studied.[1,17] Most recently, for measurements of adsorbed species or intermediates at the electrode surface, a transient mode of SECM, surface interrogation (SI)-SECM, was developed but not yet demonstrated for nm scale measurements.[15]

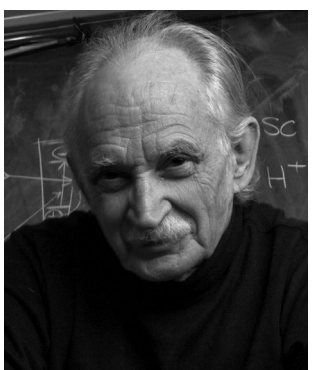

Allen J. Bard

Allen J. Bard is the Director of the Center for Electrochemistry and a Professor at The University of Texas at Austin. He has been the Hackerman-Welch Regents Chair in Chemistry since 1985. His research interests involve the application of electrochemical methods to the study of chemical problems and include investigations in scanning electrochemical microscopy, electrogenerated chemiluminescence and photoelectrochemistry. He has published over 980 peer-reviewed papers, and 76 book chapters and other publications. He has authored three books, Chemical Equilibrium (1966), Electrochemical Methods—Fundamentals and Applications (1980, 2nd edn, 2001, and Integrated Chemical Systems: A Chemical Approach to Nanotechnology (1994)).

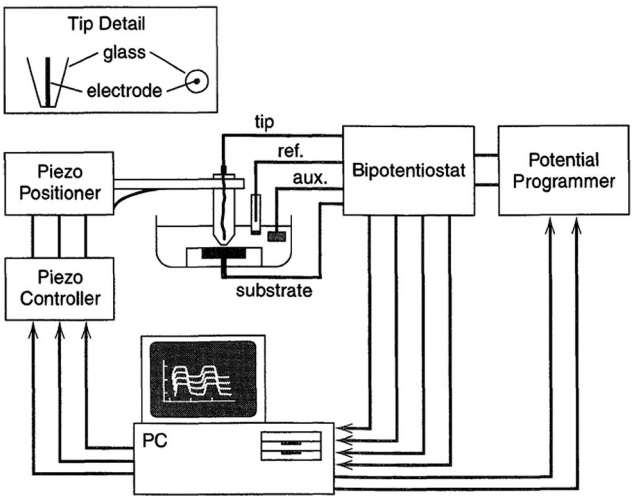

Fig. 1 Schematic description of a SECM setup. Reprinted with permission from ref. 7. Copyright 1990 American Chemical Society.

2.2.1 Feedback mode. The most frequent mode of operation of the SECM is the feedback mode, where only the tip current is monitored. Here, the tip current is perturbed by the presence of a substrate at close proximity by blockage of the diffusion of solution species to the tip (negative feedback) and by its regeneration at the substrate (positive feedback). This effect permits investigation of both electrically insulating and conducting surfaces and makes possible imaging of surfaces and the reactions that occur there. This mode of operation with surface imaging was first described in a series of papers in 1989.[1,18,19] It is also possible to carry out the same electrode reaction at the tip and substrate, called the shielding or competitive mode.[20]

In the feedback mode, as a tip approaches a comparatively large substrate in the z direction, the steady-state tip current (i_T) depends on the tip-substrate separation distance (d) and on whether the substrate is an insulator or conductor. When the tip is very far from the substrate (*e.g.*, d is greater than 10 times the tip radius (a)), the measured tip current ($i_{T,\infty}$) for the reaction O + ne → R is diffusion and mass-transfer controlled (Fig. 2a). For a disk UME, the most frequently used SECM tip geometry, $i_{T,\infty}$ is then given by eqn (1)[21]

$$i_{T,\infty} = 4nFDCa \quad (1)$$

where n is the number of electrons, F is the Faraday constant (96 500 C mol^{-1}), D is the diffusion coefficient of the redox species (cm^2 s^{-1}) in the bulk solution, and C is the redox mediator concentration (mol cm^{-3}). For $d < 10a$, the substrate affects i_T significantly. When the substrate is an insulator, the concentration of O in the tip-substrate gap decreases relative to that in the bulk solution since R generated at the tip from O in the bulk solution cannot be re-oxidized to O at the substrate and diffusion of O into the gap from the bulk solution is hindered.

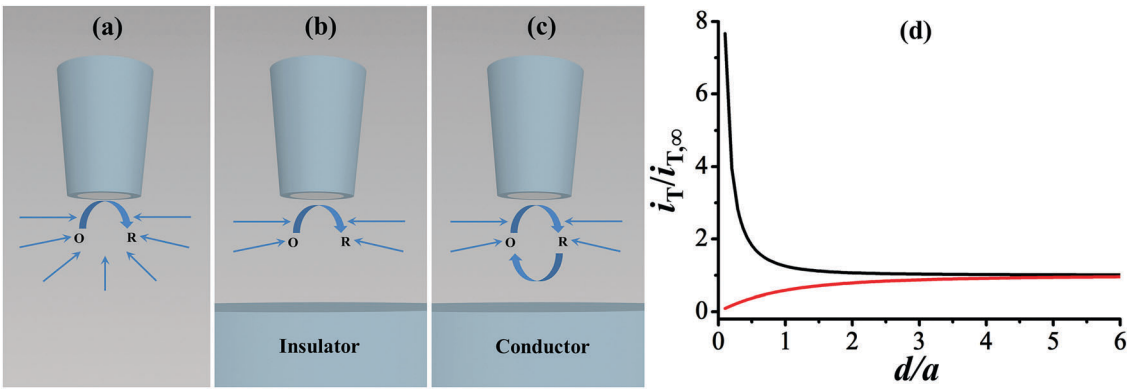

Fig. 2 SECM feedback modes. (a) Unhindered diffusion of species O in the bulk solution to a UME tip surface when the tip is far from a substrate. (b) Hindered diffusion of species O to the tip by an insulating substrate (negative feedback). (c) Increased local flux of O by a conducting substrate (positive feedback). (d) Representative negative feedback (red) and positive feedback (black) approach curves.

Thus, i_T decreases as the tip moves closer to the substrate (*i.e.*, d decreases) in this negative feedback mode (Fig. 2b). In contrast, as the tip approaches a conducting substrate, tip-generated R is re-oxidized back to O at the substrate with an increase in the local flux of O as d decreases, and a corresponding increase in i_T in this positive feedback mode (Fig. 2c). A plot of normalized current ($i_T = i_T/i_{T,\infty}$) *vs.* normalized distance ($L = d/a$) results in approach curves for either positive feedback (black) and negative feedback (red) in Fig. 2d. Since this plot involves only dimensionless variables, it does not depend on the concentration or diffusion coefficient of O. From comparison of experimental and simulated curves, one can find d from the measured i_T and also the value of $d = 0$. The approach curve for an insulator also depends on the tip RG (*i.e.*, the ratio of the tip insulating sheath radius r_g to its conducting radius a or r_g/a) since the sheath around the conducting portion of the tip also blocks diffusion, but this effect is not usually important for positive feedback.[22,23]

2.2.2 Generation/collection modes. In contrast to the feedback mode, in SECM generation/collection (G/C) modes (Fig. 3) both the tip and the substrate currents are measured. There are two modes of this type. In the tip generation/substrate collection (TG/SC) mode (Fig. 3a), the tip is used to generate a reactant that is detected at a substrate electrode. For example, the reaction O + ne → R occurs at the tip and the reverse reaction occurs at the substrate. SECM TG/SC is often used in studies of homogeneous chemical reaction rates, where the reaction of species R as it transits between tip and substrate causes a decrease in the substrate current.[24] When two or more electrochemical reactions occur on the tip at the same time, and thus two partial currents flow, the SECM multireaction TG/SC mode can be used. In multi-reaction TG/SC, two reactions occur on the tip while only one product is collected on the substrate. This permits separation of simultaneous reactions occurring on the tip.[25] An alternative mode (Fig. 3b), where the substrate is the generator and the tip is the collector (SG/TC), is used in studies of reactions at a substrate surface. The SG/TC mode was first used to study concentration profiles near an electrode surface without scanning and imaging.[26–28]

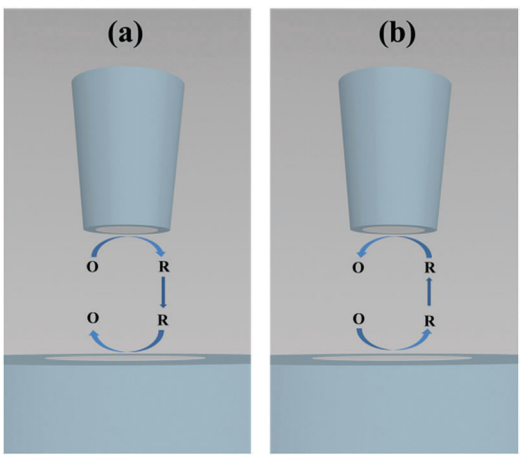

Fig. 3 SECM generation/collection (G/C) modes. (a) Tip generation/substrate collection (TG/SC) and (b) substrate generation/tip collection (SG/TC).

As discussed above, in the TG/SC mode the tip is held at a potential where an electrode reaction occurs and the substrate at a different potential where a product of the tip reaction will react and thus be "collected". In most cases, the substrate is considerably larger than the tip, so that the collection efficiency, given by i_S/i_T, where i_S is the substrate current, is essentially 1 (*i.e.*, 100%) for a stable tip-generated R. If R reacts on transit from tip to substrate, i_S/i_T becomes smaller, and its change with separation, d, permits determination of the rate constant of the homogeneous reaction. The TG/SC mode is useful in scanning arrays for screening electrocatalysts. For example, in studying the oxygen reduction reaction, one can generate oxygen at the tip at a constant current and measure how large the substrate current is for oxygen reduction (*i.e.*, how much of the oxygen is collected) as a function of substrate potential.

In the SG/TC mode, the tip probes the reactions that are occurring on a substrate. For example, a scan in the z-direction can produce the concentration profile, while a scan over the surface can identify "hot spots" where reactions occur at a higher rate. This can also be used to examine electrocatalysts.

Usually in the SG/TC mode, the collection efficiency by the tip is smaller than 1, so the system has to be calibrated with a known mediator couple.

3. Nanoscale SECM

SECM at the nm-level is challenging, and new experimental and instrumental factors must be considered. For example, the tip size and its distance from the substrate largely determine resolution. Additionally, nm-sized tips are fragile and easily destroyed by electrostatic effects and vibration. These tips are also easily contaminated, so that extremely pure solutions are essential. High positional stability is required in positioning and maintaining the tip at nm- distances. This requires a high level of control of the positioners and system temperature. However, with the development of a nm-scale SECM instrument, single reactive centers can be studied using nm-sized electrodes.

3.1 Fabrication of nm-sized electrodes

In recent years, there has been renewed interest in the fabrication, characterization, handling, and surfacing of nm-sized tips. Since it is almost impossible to polish nm-tips in the usual sense, a focused ion beam (FIB) is often used to produce a smooth surface. FIB can also be used to resurface a nm-tip. Nm-sized tips provide a resolution that is critically important in imaging and interrogation of nanosized objects such as nanoparticles adsorbed on a surface and in single molecule and single nanoparticle experiments. Advances have also been made in the ability to create nanogaps between a tip and substrate which are important in measurements of fast heterogeneous kinetics and in detecting unstable intermediates.

Key issues in the use of UMEs of submicrometer and nm-size are knowledge of their size and geometry, and whether the metal electrode protrudes from or is recessed into the insulating portion that surrounds the electrode. For electrodes with radii on the order of 70 nm or more, this can be accomplished with scanning electron microscopy (SEM). For electrodes below $\sim$50 nm, SEM often cannot be used because of resolution limitations. Steady state voltammetry can be of use in testing UME steady-state behavior. However, because such measurements do not provide information about geometry, approach curves with SECM are needed to prove that the tip is not recessed in a channel. To obtain a useful approach curve, the tip must be moved as close as one to two tip radii from the substrate, which, for a tip on the order of $\sim$13 nm, can be challenging and sometimes provides only a short, useful approach curve distance range. Small tips also imply measurements of very small currents, in the picoamp or smaller range.[29–33] Aspects of fabrication, characterization, and measurements with nanoelectrodes were recently reviewed in 2015.[6,34]

Despite their many advantages, glass-sealed metal UMEs of submicrometer and nm-size are difficult to work with due to loss of current response because of fouling. Recent studies have demonstrated that Pt tips of nm-dimension can be damaged at the nanoscale in air by electrostatic discharge (ESD) to recess the tip, which subsequently blocks the tip surface with the etched Pt and glass from the surrounding insulation (Fig. 4).[35,36] Nanoscale ESD damage can be prevented by grounding the tip and the operator, one important source of the electrostatic discharge that leads to electrochemical etching of the Pt tip. Another important contributor to ESD is when the tip is switched from the dummy cell to the potentiostat by a mechanical relay, as used in many commercial instruments at the beginning of a voltammetric or amperometric measurement. This electrochemical damage can be avoided by disconnecting the tip when the switching is carried out and then reconnecting manually once potentiostatic control of the UME is attained. A relatively high humidity ($>$30% at 20 °C) can also be helpful in preventing ESD damage.[37]

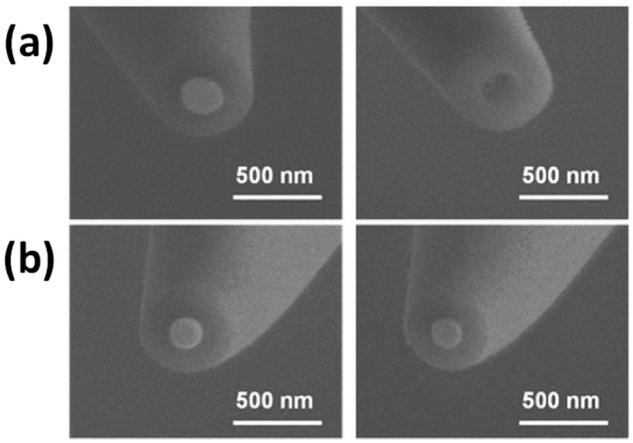

Fig. 4 SEM images of a Pt tip before (left) and after (right) a SECM experiment where the tip-substrate potential difference is (a) 400 mV or (b) 150 mV, respectively. Only the right image in (a) shows distinct nanoscale ESD damage on the Pt surface with a recess formed by electrochemical etching. Adapted with permission from ref. 36. Copyright 2016 American Chemical Society.

SECM approach curves for UME tip characterization provide valuable information regarding the metal radius (a), the insulation radius (RG) and electrode geometry, in addition to whether or not the tip is recessed or protruding. This information is crucial for the interpretation of the electrochemical measurements at these electrodes. Methods have also been developed which are useful in obtaining topographic information with nm-resolution without destruction or modification of the UME and in recognizing tips where the metal is either recessed below the insulating sheath or protruding above it. White light vertical scanning interferometry (VSI) is a noncontact optical technique that can accurately measure surface heights on a sample, and was recently used to measure nm-depths of metal recession in gold UMEs of micrometer dimension and to monitor the change in the depth of the recession after electrodeposition of gold inside the recessed hole.[38] Atomic force microscopy (AFM) has also been used to image gold and platinum UMEs of nm-dimensions in various modes, either in air or in solution.[39] Such methods allow UMEs to be used after characterization in electrochemical experiments as SECM tips or substrates.

Macroscopic and micrometer-sized solid electrodes can be reproducibly cleaned by mechanical polishing. In contrast, even very gentle polishing can dramatically change the nanoelectrode size and geometry so that replication of nanoelectrochemical experiments is difficult. Cleaning a nanoelectrode by immersion in a piranha solution or organic solvent is also not always effective. Air plasma cleaning is a possibility for non-destructive cleaning of nanoelectrode surfaces.[40] AFM images and electrochemical measurements taken before and after the plasma cleaning indicate that the air plasma cleaning is effective in removing impurities and polymer films from the electrode surface.

Because of difficulties in fabrication, maintenance, stability, and lifetime of UMEs of nm-size, making larger, robust electrodes that still provide comparable nm-gaps is possible. There are two recent examples of such electrodes. In the first, a Pt UME of radius 5 μm was fabricated with a rounded (truncated hemispherical) metal tip and insulating glass sheath with RG $<$ 1.1, as shown in the SEM Fig. 5a.[41] With this electrode, the normalized tip current, $i_T(L)$, was enhanced by a factor as high as 30 times the magnitude of its limiting current in bulk solution at closest approach, corresponding to a tip-substrate gap of about 115 nm as shown in Fig. 5b. The tip geometry and tip-substrate distances were characterized by fitting the approach curve based on positive feedback from a Pt substrate. A good fit was found between the experimental and theoretical curves, simulated by considering the exact shape of the glass sheath and metal tip as found from the SEM image.

In the second example, a nanoelectrode with high sensitivity by means of blocking the conducting surface of a UME with a thin insulating TiO_2 layer ($\sim$1 nm thick) that allows tunneling to a NP, was developed.[42,43] When that layer was thin enough such that tunneling to NPs could occur, this electrode was used to capture a single metal NP in a collision experiment. This NP on an otherwise insulating surface in effect created a nanoelectrode with enhanced sensitivity and very low background current, since the charge transfer reaction to a solution species occurred solely *via* the NP. The fabrication approach is shown in Fig. 6a and b. The resulting tunneling ultramicroelectrode (TUME) has a geometry defined by the attached NP (Fig. 6c, inset) and can be used as a SECM tip (Fig. 6c) with an approach capability within 1–2 nm of substrate contact. The TUMEs have many potential applications, including their use as probes in high resolution SECM or as nanoelectrodes for kinetic investigations. The construction of TUMEs may also provide a direct electrochemical means of investigating the reactivity of individual metal NPs or of characterizing the band structure of thin insulator/semiconductor films electrochemically.

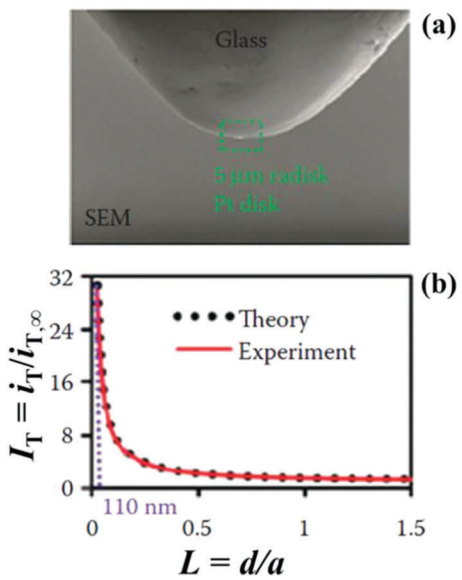

Fig. 5 (a) SEM image of a 5 μm-radius Pt tip with a thin-glass sheath, RG $<$ 1.1, and (b) a positive feedback approach curve obtained by carefully aligning the Pt tip over the highest point of a Pt substrate. Adapted with permission from ref. 41. Copyright 2011 American Chemical Society.

3.2 Nano SECM instrumentation

Imaging at the nm-level is not trivial and a number of new factors are important in designing a nano SECM instrument. Tip size and tip distance from the surface are the determining factors for the overall resolution. Nm-sized tips are fragile and susceptible to damage by electrostatic discharge (ESD) and vibration, as discussed previously (Fig. 4). These tips are also easily contaminated so that extremely high purity solutions are critical.[36,37,44] Because the tip in SECM never directly contacts the surface, nm-tip positioning and maintenance at nm-distances require a high level of tip positional stability.[36,37,45] In addition to nm-control of the tip, thermal stability of the system is required. The nanoscale SECM designed by our group (Fig. 7) not only focused on improving imaging resolution but also on improving tip positioning over a level of tens of nanometers without direct contact with a substrate.[36,37] This latter capability enables the measurement of extremely fast kinetics with significantly enhanced mass transfer rates. Two requirements that are critical in performing SECM with nm-scale resolution and high positional stability in the z direction, as well as for lateral resolution for imaging include (1) suppressing thermal drift and (2) preventing potentiostat induced tip damage at nanoscale distances. These requirements involve the construction and the modification of the software and instrumentation hardware for nanoscale SECM, including: (1) software code developed to synchronize the SECM tip movement (*i.e.* positioning system in Fig. 7) with electrochemical response (*i.e.*, electrochemical system in Fig. 7), (2) the construction of an isothermal chamber to stabilize the nm-scale gap between the tip and substrate, (3) the modification of a commercial bipotentiostat to avoid electrochemical tip damage during SECM experiments, and (4) the construction of an SECM stage to avoid artifacts in SECM images. Each of these is described briefly below.

3.2.1 Synchronizing SECM tip movement with electrochemical response. The instrument has a bipotentiostat and a stage equipped with piezoelectric actuators operated with custom (LabVIEW) software. Software was written to interface and synchronize the tip motion with the measured tip current from the bipotentiostat. This separation of the tip positioning

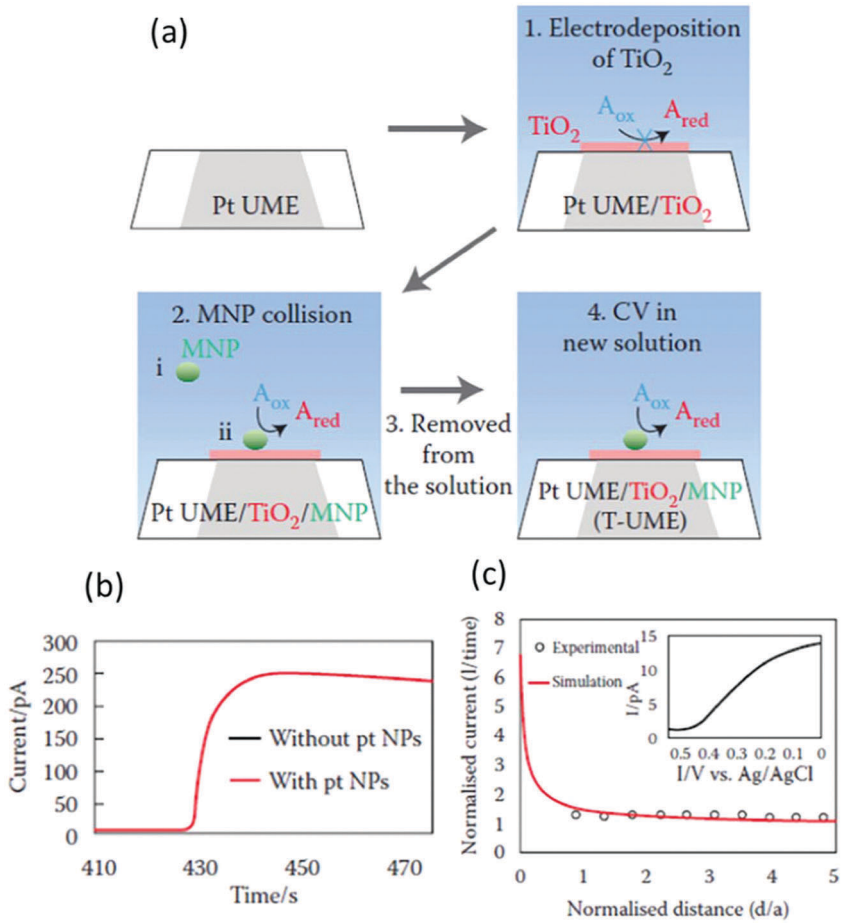

Fig. 6 (a) Fabrication of a tunneling UME (TUME) by electrodeposition of TiO_2 on a Pt UME, attachment of a metal NP through collision, removal of UME from the solution, CV or SECM experiments in a new solution. (b) Chronoamperometric curve for attachment of a PtNP at the TiO_2-deposited Pt UME in 10 mM $K_3Fe(CN)_6$ with (red) and without (black) 120 pM Pt NPs. Data acquisition time: 50 ms at constant potential = −0.6 V *vs.* Ag/AgCl. (c) Positive feedback approach curve over a glassy carbon wafer in 10 mM $K_3Fe(CN)_6$/70 mM KCl (open circles) fitted with theory based on a spherical NP of 5 nm diameter on a UME insulated surface (red line). E_{tip} and $E_{substrate}$: −0.2 and 0.6 V *vs.* Ag/AgCl, respectively. Inset: Tip voltammogram in the bulk solution. Adapted with permission from ref. 42. Copyright 2014 American Chemical Society.

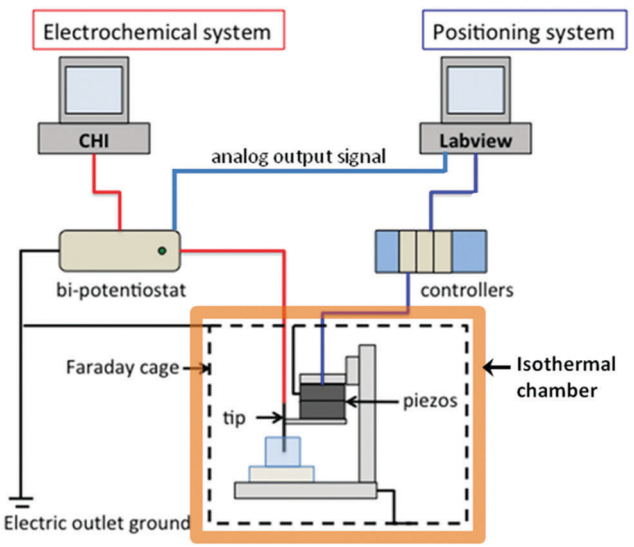

Fig. 7 Schematic diagram of nanometer scale SECM. Reprinted with permission from ref. 37. Copyright 2016 American Chemical Society.

control system from the electrochemistry using two different circuits and computers (Fig. 8) was done to avoid any possible conflicts between the two different software. The first computer operates the bipotentiostat (left computer in Fig. 7) while the second computer (right computer in Fig. 7) uses a custom-developed program to control the movement of the piezos and synchronizes their movement with the tip current by reading the analog output signal from the bipotentiostat through a data acquisition board.[36] A single ground was used to avoid any ground loop issues and all conducting parts in the isothermal chamber and the electronic equipment were grounded to protect the SECM tip electrode from ESD damage.

3.2.2 Isothermal chamber construction. An isothermal chamber (Fig. 8) is necessary to stabilize the nm-scale gap between the tip and substrate as described previously.[36,45] The SECM stage is placed within the isothermal chamber, where a constant temperature of 24 °C is maintained. Highly precise piezo (x,y,z) positioners incorporating a capacitive sensor placed inside each stage were used, thus enabling control of their motion with a resolution of 0.2 nm. A lockable,

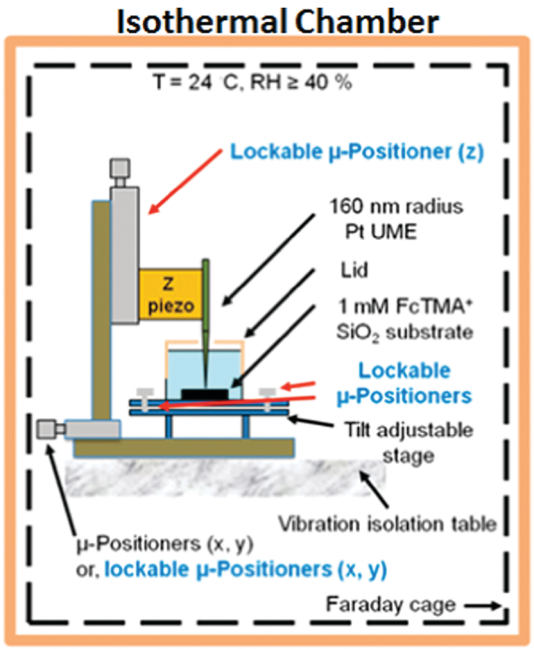

Fig. 8 SECM stage placed in an isothermal chamber. Adapted with permission from ref. 36. Copyright 2016 American Chemical Society.

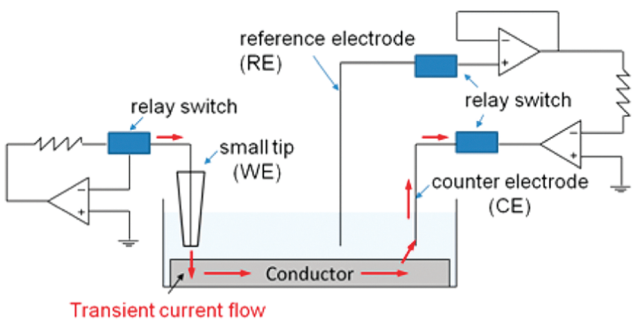

Fig. 9 Possible flow of the transient current from a working electrode amplifier to a Pt tip, to a conductive substrate, and finally to a counter electrode. Red arrows depict transient current flow. Adapted with permission from ref. 36. Copyright 2016 American Chemical Society.

manual coarse-positioner was also used to keep the thermal drift in the z direction <0.5 nm min^{-1}.

3.2.3 Commercial bipotentiostat modification. A commercial bipotentiostat (CH Instruments) was modified by removing mechanical relays and replacing them with manual switches to avoid electrochemical damage to the nm-size tip during SECM experiments, especially for a tip positioned near a conductive substrate where a transiently charged tip can discharge through current flow through the substrate (Fig. 9).[36]

3.2.4 Construction of an SECM stage to avoid artifacts in SECM images. All tip x, y coarse micro (μ)-positioners and stage μ-positioners, *e.g.* stepping motors, were replaced by lockable manual μ-positioners in order to eliminate distortion in SECM images when scanning laterally (Fig. 10).[36] For nanoparticle imaging, for example, SECM images that reflect a spherical geometry (Fig. 10a and b) in agreement with SEM images and simulations, are obtained, compared to ellipsoidal-shaped SECM images (Fig. 10c and d) in the absence of lockable μ-positioners.

4. Applications

4.1 Nanogap applications

4.1.1 Measurements of rapid homogeneous reactions and short-lived intermediates. A nm gap (10–500 nm) between the SECM tip and substrate, where an electrode reaction is carried out at a tip (generator) and intermediates collected at a substrate with the TG/SC mode, is being used in studies of extremely fast reactions. This is because the time (τ) required for intermediates to travel across the gap of dimension, δ, is

$$\tau = \delta^2/(2D) \quad (2)$$

where D is the diffusion coefficient. Thus, for $D = 10^{-6}$ cm^2 s^{-1}, gaps of 1 μm, 500 nm, 100 nm, and 50 nm yield τ-values of about 5 ms, 1.25 ms, 50 μs and 12.5 μs, respectively. Since the time required for intermediates to cross a nanogap of 100 nm or less is on the order of microseconds, intermediates can arrive at the substrate without further reaction. Unlike fast-scan cyclic voltammetry (FSCV),[46] SECM measurements are conducted at steady state, where charging current does not occur. Moreover, generation and collection of an intermediate are carried out with two separate electrodes, so that adsorbed species on the tip electrode do not interfere with its collection. Different collection efficiencies obtained with different nanogap distances facilitate the analysis of the life-time of an intermediate, and also the kinetics parameters for following homogeneous reactions.

Since the earliest work in 1994 by the TG/SC mode for the detection of acrylonitrile anion radical in DMF in investigating the dimerization to ultimately yield adiponitrile with a μm gap,[47] a number of other similar studies have been reported. These include guanosine oxidation[48] and the formation of *N*,*N*-dimethylaniline (DMA) cation radicals in the benzidene rearrangement[49] in aprotic solution. In addition, Sn(III)[50] and superoxide[51] intermediates in aqueous solution have been detected. For DMA cation radical detection, the oxidation of DMA was accomplished in acetonitrile (MeCN) with 0.1 M tetra-*n*-butylammonium hexafluorophosphate ($TBAPF_6$). As indicated in Fig. 11a, a 500 nm radius Pt UME was used for the generation of DMA$^{\bullet+}$, which can either dimerize into tetramethylbenzidene (TMB) or be collected at the substrate (a 5 μm radius Pt UME). The collection currents of DMA$^{\bullet+}$ at different gap distances are shown in Fig. 11b, where a collection efficiency (CE) of 90% can be obtained at a gap distance of 200 nm, indicating that almost all DMA$^{\bullet+}$ was collected by the substrate without further reaction. By fitting the experimental data, a dimerization rate constant of 2.5×10^8 M^{-1} s^{-1} was found.

Recently, detection and characterization of $CO_2^{\bullet-}$ during CO_2 reduction in DMF was accomplished (Fig. 12a) using SECM.[52] A 5 μm radius hemispherical Hg/Pt UME was used as the SECM tip to reduce CO_2, and the collection of $CO_2^{\bullet-}$ was

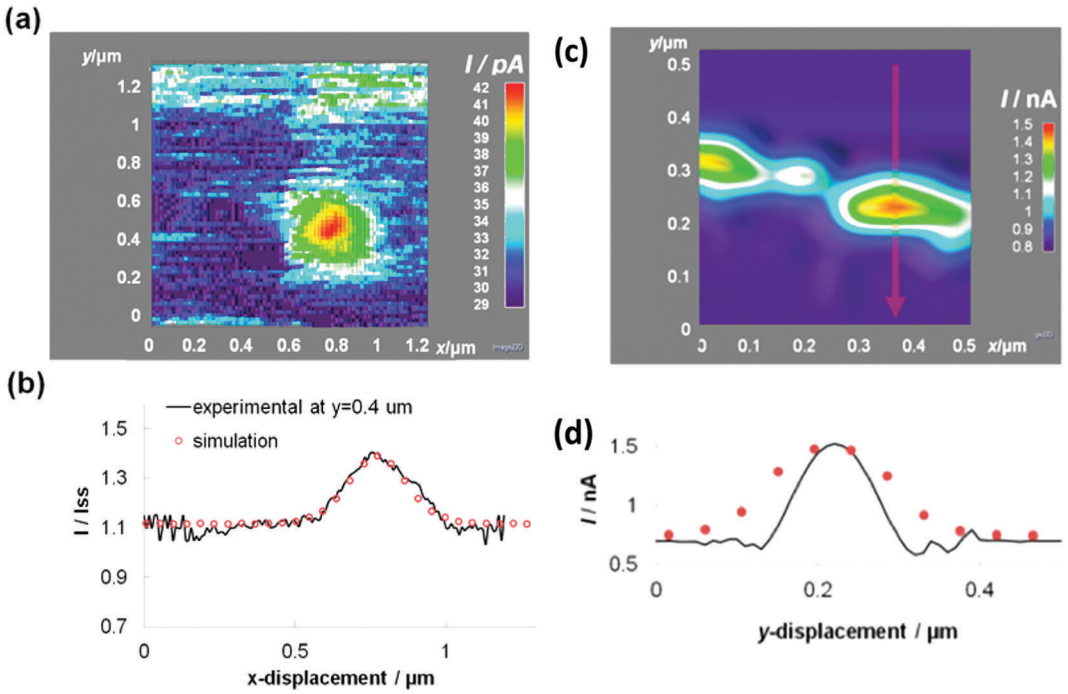

Fig. 10 (a) SECM image of an individual Pt NP obtained in 1 mM $FcTMA^+$/10 mM $NaClO_4$ after replacing both *x*- and *y*-unlockable μ-positioners with lockable μ-positioners. E_{tip} = 0.3 V, $E_{substrate}$ = −0.1 V *vs.* Pt QRE; Pt UME scan rate: 200 nm s^{-1} (20 nm incremental distance per 0.1 s incremental time). (b) Cross-section current responses along y = 0.4 μm from the SECM image in (a). Experimental curves (solid lines) fit well with theoretical simulation (circles) in terms of current magnitudes, where the electron transfer reaction at Pt NPs is governed by diffusion control in this analysis. Good agreement between two data sets is seen in current peak width proving the image is from a single NP. (c) SECM image of the hydrogen oxidation reaction in 2 mM $HClO_4$, 10 mM $NaClO_4$ at Pt NPs. E_{tip} = −1.0 V, $E_{substrate}$ = −0.4 V *vs.* Pt QRE. Tip scan rate: 200 nm s^{-1}. (d) Cross-section current responses along the red arrow from the SECM image in (c). Maximum current magnitude in experimental curves (solid lines) agreed well with that in the theoretical simulation (circles). In this analysis, the ET reaction at Pt NPs is controlled by diffusion. A discrepancy, however, exists in current peak width. Adapted with permission from ref. 36. Copyright 2016 American Chemical Society.

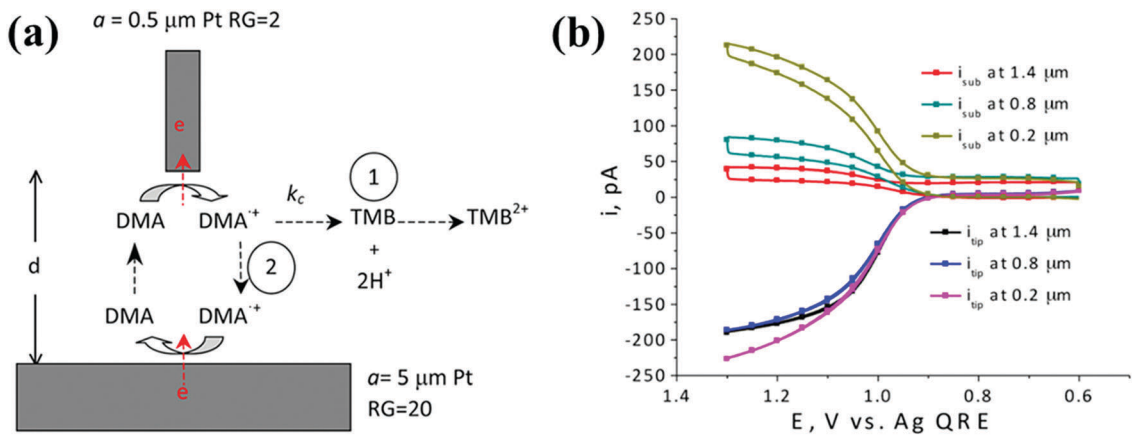

Fig. 11 TG/SC mode for the detection of $DMA^{\bullet+}$ radical. (a) Schematic of the collection of the unstable $DMA^{\bullet+}$ radical. The generated $DMA^{\bullet+}$ can either dimerize into TMB, route 1, or be reduced by the substrate, route 2. (b) At the gap distance of 1.4 μm, 0.8 μm and 0.2 μm, the oxidation of 0.4 mM DMA was conducted at the tip by sweeping the tip potential from 0.6 V to 1.3 V (bottom). The collection of $DMA^{\bullet+}$ radical was achieved by holding the substrate potential at 0.76 V *vs.* Ag QRE (top). Adapted with permission from ref. 49. Copyright 2014 American Chemical Society.

accomplished at a 12.5 μm radius Au UME at different gap distances (Fig. 12b). In this study, the final product, oxalate, was also detected quantitatively. The dimerization rate constant of 6.0×10^8 M^{-1} s^{-1} was obtained by fitting the experimental data with the theoretical simulation. A significant difference in the heterogeneous rate constant at different quaternary ammonium electrolytes was also observed and was attributed to a "tunneling effect" caused by the adsorption of the electrolyte on the electrode surface at negative potentials with respect to the potential of zero charge (PZC). The ability to

quantitatively measure $CO_2^{\bullet -}$ in aprotic solution within the nanogap provides the possibility of utilizing SECM as a tool to conduct mechanism studies for CO_2 reduction with heterogeneous and homogeneous catalysts.

Mirkin and coworkers recently developed a method for the determination of superoxide radical anion ($O_2^{\bullet -}$) at a nanoscale liquid–liquid interface during oxygen reduction at a Pt surface in aqueous solution.[51] A nanopipette, which was filled with benzotrifluoride saturated with oxygen, approached the Pt substrate in aqueous solution. Oxygen from the organic filling solution diffused into the external aqueous phase and was reduced at the Pt substrate. The generated superoxide intermediate diffused back to the organic phase at the very small gap distance ($d \leq 50$ nm). The measured ion transfer current, which was attributed to the superoxide intermediate, was observed. The pseudo-first-order rate constant, k_c, was determined to be 3.4×10^5 s^{-1}. Since the distance between the nanopipette and the substrate can be extremely close (*e.g.*, 1 nm) without incurring electron tunneling, the authors speculated that extremely short-lived intermediates with a lifetime of only a few nanoseconds can be captured with this approach.

4.1.2 Measurements of heterogeneous electron transfer kinetics. Nanogap-SECM can also be used to study fast heterogeneous reaction kinetics due to the relative extremely fast mass transfer that is possible as a result of a nanometer tip-substrate separation distance. For accurate determination of the heterogeneous rate constant (k^0), the mass transfer rate, which is proportional to D/d, must be large compared with k^0.[53] This means that a larger k^0 can be measured with a smaller tip-substrate distance. For example, Mirkin and co-workers reported a k^0 of 17 cm s^{-1} for $Ru(NH_3)_6^{3+}$ reduction at a Pt nanotip above a Au substrate with d = 15 nm.[30] Moreover, the kinetics of tris(2,2′-bipyridine)-ruthenium(II) (Ru(bpy)) oxidation and reduction were investigated at tip-substrate distances ranging from 2 μm to 450 nm.[54] As an important molecule for ECL, it can serve as either an electron donor or acceptor (Fig. 13a). As indicated in Fig. 13b, the steady-state voltammograms for Ru(bpy) oxidation become increasingly less reversible with decreasing d, as heterogeneous kinetics become more significant relative to mass transfer. From the tip voltammograms, k^0 was estimated to be 0.7 ± 0.1 cm s^{-1}. This slower k^0 was attributed to the blocking effect of the 2,2′-bipyridine ligands during oxidation of the ruthenium(II) center. In contrast, reduction of the ruthenium(II) center involves electron transfer to the exposed ligands, resulting in the lower limit for k^0 of 3 cm s^{-1}.

Macroscopic substrates with different electrochemical properties have also been investigated by SECM nanogap voltammetry. For example, Amemiya and co-workers developed a method for the study of organic contamination of a HOPG surface by quantitatively monitoring its electrochemical activity to the kinetically fast redox couple $FcTMA^+$.[44] SECM-based nanogap voltammograms show that faster kinetics for the redox couple $FcTMA^{2+/+}$ was obtained at the HOPG surface, as the aqueous concentration of organic impurities was decreased from ~20 to ~1 ppb. This result indicates that an organic layer, which depends on the water used and ambient air, was adsorbed on the HOPG surface. Their later work demonstrated that the contamination of the HOPG surface can be alleviated when HOPG is exfoliated in humidified air to form a nanometer-thick water adlayer.[55] However, Unwin and coworkers disagreed and suggested that "reversible adsorption/desorption" could play a role during the nanogap measurements because the time required to reach steady-state increases if adsorption/desorption takes place.[56,57] They further mentioned that the effect of interfacial charge on mass transport and double layer effects

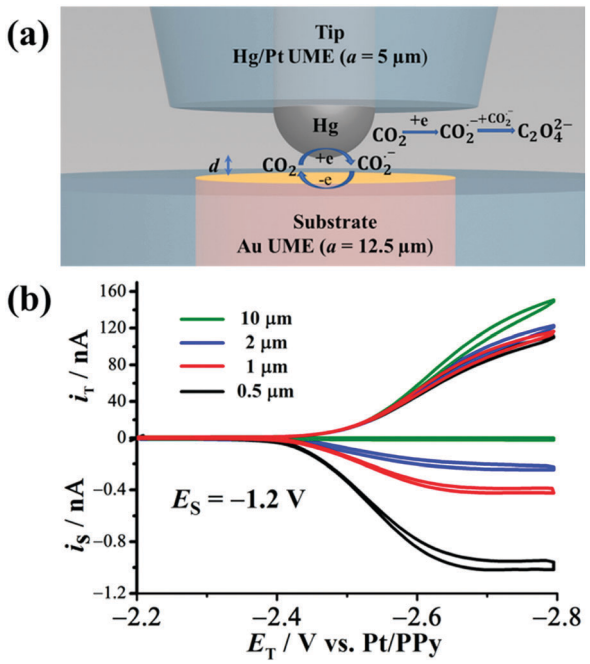

Fig. 12 Collection of the $CO_2^{\bullet -}$ radical in the SECM TG/SC mode. (a) CO_2 was reduced at a hemispherical Hg/Pt UME (a = 5 μm). Oxalate was generated by $CO_2^{\bullet -}$ dimerization at the upper portion of the hemisphere, whereas at the lower portion of the hemisphere, $CO_2^{\bullet -}$ was captured by the SECM substrate (*e.g.*, a a = 12.5 μm Au UME). (b) Collection curves of 20 mM CO_2 reduction in DMF at a gap distance of 10, 2, 0.5, and 0.05 μm, respectively. The tip potential was swept from −2.2 V to −2.8 V at a scan rate of 100 mV s^{-1} to reduce CO_2, while the substrate potential was held at −1.2 V *vs.* Pt/PPy to collect $CO_2^{\bullet -}$. Adapted with permission from ref. 52. Copyright 2017 American Chemical Society.

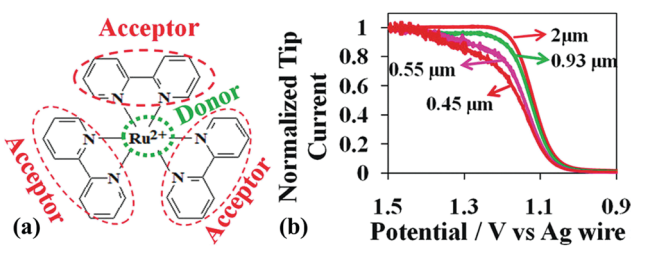

Fig. 13 Ru(bpy) molecule (a) and normalized steady-state voltammograms (b) obtained at a SECM tip (a Pt UME) for 0.38 mM Ru(bpy) oxidation at different gap distances in acetonitrile/0.1 M $TBAPF_6$. Adapted with permission from ref. 54. Copyright 2011 American Chemical Society.

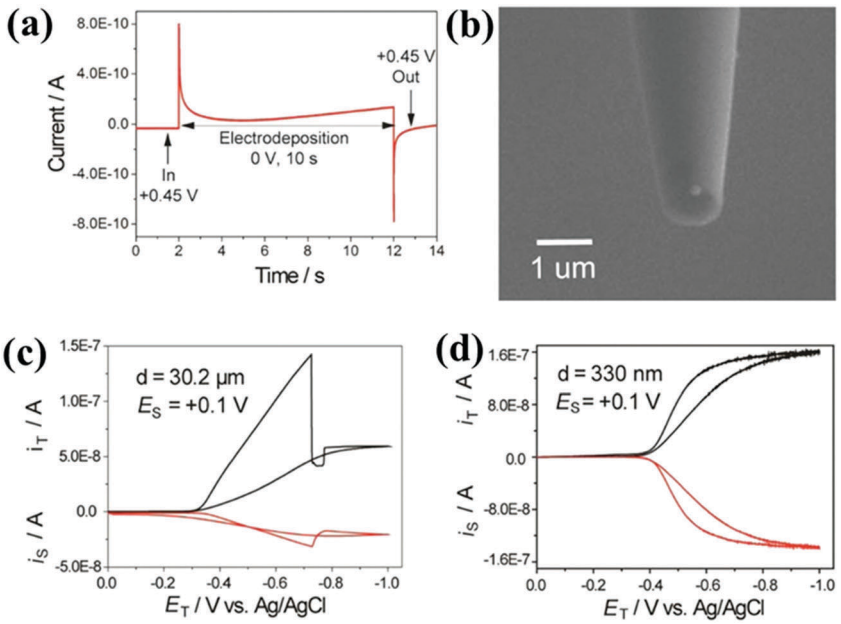

Fig. 14 Current–time response (a) of a single Pt NP deposit on a carbon UME in 100 μM H_2PtCl_6 solution containing 10 mM H_2SO_4. (b) The SEM image of a Pt NP attached to carbon UME after electrodeposition. H_2 was generated at the tip (black curves in c and d) and collected at the substrate (red curves in c and d) with TG/SC mode of SECM at gap distances of 30.2 μm (c) and 330 nm (d), respectively. E_T: scanned from 0 to −1 V at a scan rate of 100 mV s^{-1}. E_S: 0.1 V *vs.* Ag/AgCl. Adapted with permission from ref. 58. This is an unofficial adaptation of an article (ref. 58) that appeared in an ACS publication. ACS has not endorsed the content of this adaptation or the context of its use.

need to be considered for kinetic analysis by SECM nanogap experiments.

4.1.3 Other nano-gap studies. In addition to studies of homogeneous and heterogeneous reactions, measurements of the size of NPs and clusters attached on the electrode surface have also been conducted within the nanogap.[58] For example, a single Pt NP or NP clusters were electrodeposited on carbon nanoelectrodes, as shown in Fig. 14a and b. The size of the Pt NPs and clusters can be deduced from the steady-state currents obtained from the hydrogen evolution reaction (HER) on the Pt NPs and clusters but not on the carbon substrate at the given potential. However, the generation of H_2 bubbles on the Pt NPs and clusters was observed and prevented size determination (Fig. 14c). Nanogap SECM was introduced to prevent H_2 bubble formation, as indicated by the well-defined steady-state voltammograms obtained on both the SECM tip and substrate (Fig. 14d). Through this approach, Pt NPs and clusters size down to 1 nm dimensions can be measured.

4.2 Nano-SECM imaging

As a scanning probe technique, SECM is uniquely able to provide both chemical and topographic information of a surface immersed in a solution.[2] We describe here the recent nm SECM imaging in studies of electrocatalytic activities of single nanoparticles (NPs)[37,59–61] and topographic and electrochemical imaging of biological cells.[62,63] In addition, SECM combined with other techniques (*e.g.*, AFM and scanning ion conductive microscopy (SICM)) for topographic and chemical imaging with submicrometer resolution was also demonstrated.[16,64]

4.2.1 Single nanoparticles (NPs). The catalytic activity of individual spherical Pt NPs for the hydrogen oxidation reaction (HOR) was investigated.[37] Pt NPs with a few tens to a hundred nm radius was electrodeposited on highly oriented pyrolytic graphite (HOPG) *via* a nucleation and growth mechanism in the absence of capping agents and anchoring molecules (Fig. 15a). A focused ion beam (FIB)-milled Pt nanoelectrode (90 nm radius, Fig. 15b) was fabricated for SECM imaging of Pt NPs on HOPG using the constant distance mode. The topography of the individual NPs (Fig. 15c) was obtained using an out-sphere redox mediator, $FcTMA^+$, while the catalytic activity of individual NPs was demonstrated with the HOR (Fig. 15d), within the stable nm gap generated between the tip and substrate. A lower limit of the heterogeneous rate constant of 2 cm s^{-1} for the HOR reaction was obtained at each Pt NP. By fitting the experimental results with the simulated ones, the spatial orientation, shape and catalytic activity of each NP were obtained. This approach should be useful for the analysis of the catalytic activity of a variety of individual metal NPs. The capping agent effects on the catalytic activity of NPs could also be evaluated.

Similarly, the electrocatalytic activity of other NPs was also demonstrated. For example, Mirkin and co-workers studied the hydrogen evolution reaction (HER) on individual Au NPs in SG/TC mode.[59] An SECM image of a spherical Au NP on the carbon surface with the spatial resolution of ~6 nm was obtained using an extremely small (~3 nm radius) polished Pt nanoelectrode. Recently, an image of a Pd nanocube on the HOPG/polyphenylene surface was obtained with a 10 nm radius Pt nanoelectrode using a 1 mM Fc solution in the feedback

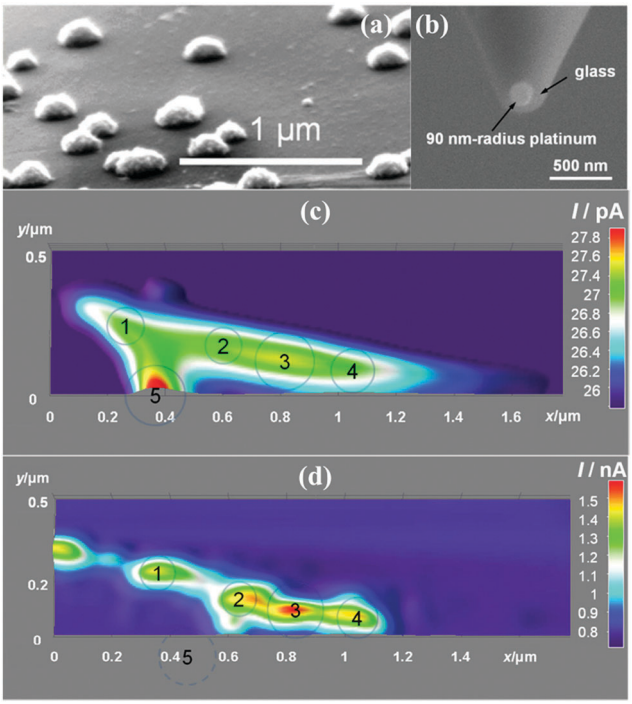

Fig. 15 (a) Side view of the field emission-scanning electron microscopic (FE-SEM) image of electrodeposited Pt NPs on HOPG. (b) SEM image of a FIB milled Pt nanoelectrode. (c) SECM image of Pt NPs obtained with a 90 nm radius Pt nanoelectrode using 1 mM $FcTMA^+$ at a tip height of 210 nm above HOPG substrate, with E_{tip} = 0.3 V, $E_{substrate}$ = −0.1 V *vs.* Pt QRE. (d) SECM image of HOR reaction at Pt NPs obtained at a tip height of 134 nm. The tip was scanned at 200 nm s^{-1} for (c) and (d). Adapted with permission from ref. 37. Copyright 2017 American Chemical Society.

mode.[60] A sharp rectangular shape of the nanocube with a high lateral resolution (on the order of 1 nm) was observed and was attributed to direct electron tunneling between the tip and the Pd nanocube.

The authors believe that this tunneling mode of nano SECM could become an important approach to achieve high-resolution imaging of single NPs.

4.2.2 Single biological samples. SECM has been applied to the study of a variety of biological samples (*e.g.*, DNAs, proteins, membranes, and cells) for a long period of time.[2] However, at nanoscale resolution, SECM imaging is still challenging. The first SECM topographic images of biological samples, such as fragments of DNA, keyhole limpet hemocyanin, mouse monoclonal immunoglobulin G (IgG) and glucose oxidase, on a mica surface were reported by Fan and Bard.[65] As shown in Fig. 16a, a thin layer of water with a thickness of sub-nanometers forms on the mica surface in humid air. A sharp and uninsulated tungsten tip was used as the SECM tip. When the tip contacted the thin water layer, a faradaic current of ∼1 pA was obtained at the tip, indicating a contact radius of less than 3 nm. Negative feedback was observed when the tip was in the vicinity of the mica and the target biological molecules, which enabled topographic imaging in the constant current mode, where the tip-mica distance was monitored. The image of the fragments of DNA molecules (Fig. 16b) on mica was obtained by holding the tip potential at 3 V at 80% relative humidity. IgG molecules on the mica were imaged in the similar way (Fig. 16c). A lateral resolution of ∼1 nm was achieved and the shapes of these molecules were similar to those determined from other established methods (*e.g.*, tunneling electron microscopy (TEM)). Recently, Mirkin and coworkers reported the topographic images of a human breast epithelial (MCF-10A) cell with a spatial resolution of ∼100 nm, which was obtained using a membrane-impermeable molecule, $Ru(NH_3)_6^{3+}$, as the redox mediator in the negative feedback mode.[62]

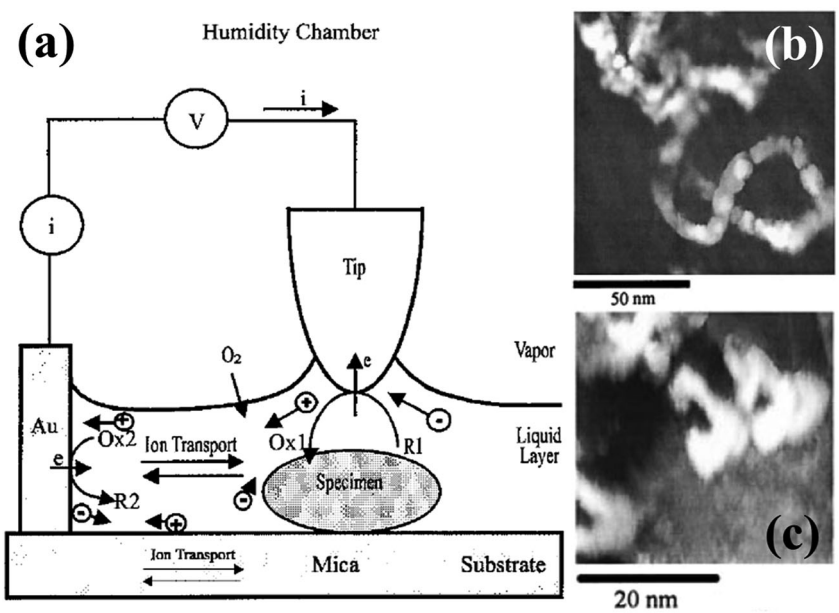

Fig. 16 (a) Schematic description of the SECM setup for single biological sample imaging with controlled humidity. The images of the fragment of DNA (b) and IgG (c) were obtained in the constant current mode. Adapted with permission from ref. 65. Copyright 1999, the National Academy of Science, USA.

A chemical flux across a cell membrane was also measured with SECM. For example, the flux of FcMeOH at the confluent monolayer of epithelial cells was monitored using a 300 nm radius Pt nanoelectrode.[66] The same electrode was used to generate hydroxide ions in the vicinity of the individual cells.[67] Cell apoptosis was observed by monitoring the topographic change of a single cell by SECM. The characterization of the redox state of intracellular unstable species was accomplished with a platinized nanoelectrode. This nanoelectrode can penetrate through the cell membrane, without affecting the physiological activity of the cell, for the measurement of concentrations of the reactive oxygen and nitrogen species (ROS and RNS) in nontransformed and metastatic human breast cells.[68,69]

SECM was applied to the measurements of the distribution of membrane protein on single cells. For example, in order to evaluate the expression level of epidermal growth factor receptor (EGFR) on A431 cells, EGFR was labeled with an alkaline-phosphatase-tagged antibody. The redox mediator, *p*-aminophenol (PAP), was produced by an ALP-catalyzed reaction. By measuring the oxidation current of PAP, the amount of EGFR on the cell surface could be estimated.[70] More importantly, the simultaneous measurement of both topography and EGFR distribution of A431 cells was achieved using a voltage-switching mode of SECM (VSM-SECM).[63] As shown in Fig. 17a, initially, a negative potential (−0.5 V *vs.* Ag/AgCl) was applied for the reduction of $Ru(NH_3)_6^{3+}$ on a 720 nm radius carbon-filled nanoelectrode. The tip was approached toward the cell surface, and a decreased current was observed because of hindered diffusion (left). The tip potential was subsequently switched to +0.35 V *vs.* Ag/AgCl to detect PAP (right). Then, the tip was withdrawn from the cell surface and moved to another preset position for another measurement. Through this approach, the topographical image of A431 cells (Fig. 17b) and distribution of EGFR on the cell membrane (Fig. 17c) were obtained synchronously. Although the spatial resolution of the images is limited by the size of the SECM tip utilized here, the VSM-SECM mode still provides the opportunity to precisely measure the chemical event occurring on the cell membrane at nanoscale resolution and is relevant to biological, physiological and biochemical studies.

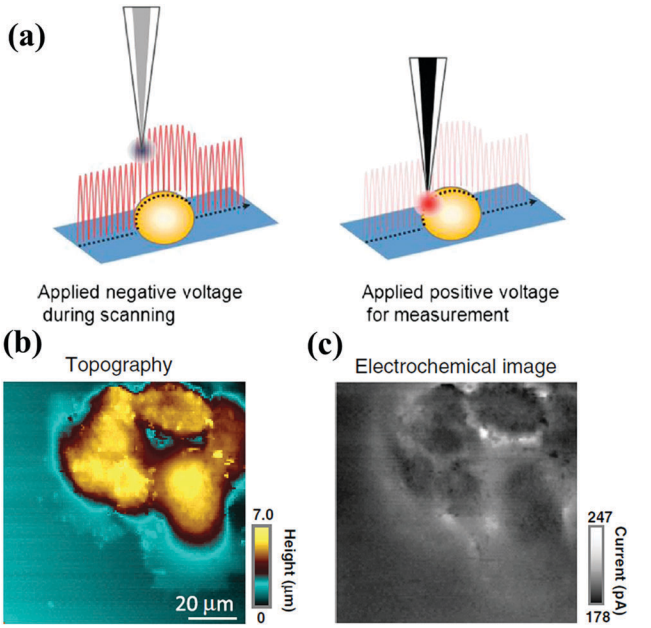

Fig. 17 (a) Schematic description of VSM-SECM. The topography of the surface was obtained from the signal for hindered diffusion of a mediator in the hopping mode (left), whereas the electrochemical measurements were conducted after switching the voltage at each data point, as shown on the right. Topographic (b) and electrochemical (c) images of A431 cells obtained in Hepes buffer containing 10 mM $Ru(NH_3)_6Cl_3$ and 4.7 mM PAPP. The SECM tip (720 nm radius carbon electrode) was held at −500 mV and 350 mV *vs.* Ag/AgCl to obtain topography and electrochemical activity of the cells, respectively. Adapted with permission from ref. 63. Copyright 2012, The National Academy of Science, USA.

4.2.3 Combined techniques. Different techniques (*e.g.*, AFM and SICM) can be combined with SECM for nanoscale imaging. For SECM-AFM, a feedback loop controlled by a computer was used to keep the cantilever amplitude constant. Thus, the gap distance was kept constant while the tip was scanned across the surface. A good example is the work by Demaille and co-workers, who fabricated a conductive SECM-AFM tip for the simultaneous measurement of the topographic and electrochemical properties of individual ~20 nm gold nanoparticles modified with a ferrocene/poly(ethylene glycol) (Fc/PEG) capping agent.[71] The same system was extended to the *in situ* mapping of the distribution of proteins on an individual virus.[72] Also, a Pt-coated AFM cantilever was fabricated for topographic imaging of a nanoporous polycarbonate membrane, while the diffusional transport of $IrCl_6^{3-}$ through the nanopores was imaged simultaneously.[73] A pre-coated Pt layer at the tip portion of an AFM cantilever probe was electrically insulated with SiO_2 except at the very apex of the tip. The fabricated probe was utilized for the electrochemical image of Pt lines using 5 mM $Ru(NH_3)_6Cl_3$ in the constant distance mode where a high spatial resolution of ~10 nm was achieved.[74] The topography and electrochemical activity of the graphene and graphite flakes exfoliated from HOPG were also evaluated with SECM-AFM.[75] Despite the extensive studies mentioned above, the intrinsic disadvantage for the SECM-AFM measurement is that the imperfect geometry of the SECM-AFM tip makes quantitative electrochemical measurements difficult.

Alternatively, SICM was integrated with SECM for nanoscale topographic and electrochemical imaging of various substrates (*e.g.*, metal pattern,[76] nanopore[77] and biological cells[78,79]). SICM is another non-contact SPM technique, which provides a constant gap distance for constant-distance SECM imaging. For example, a double-barrel carbon nanoprobe (DBCNPs, Fig. 18a) was fabricated for topographic imaging of the differentiated P12 cells (Fig. 18b). A neurite with a width of ~100 nm was observed. The cell membrane was stimulated with K^+ ion, released by the SECM-SICM probe, and the subsequently generated neurotransmitter from the cell was detected by the same probe over the cell surface (Fig. 18c). Similarly, a nanocapillary/nanoring electrode with a diameter of 330 nm was fabricated as the SECM-SICM probe for topographic and electrochemical imaging of Pt bands

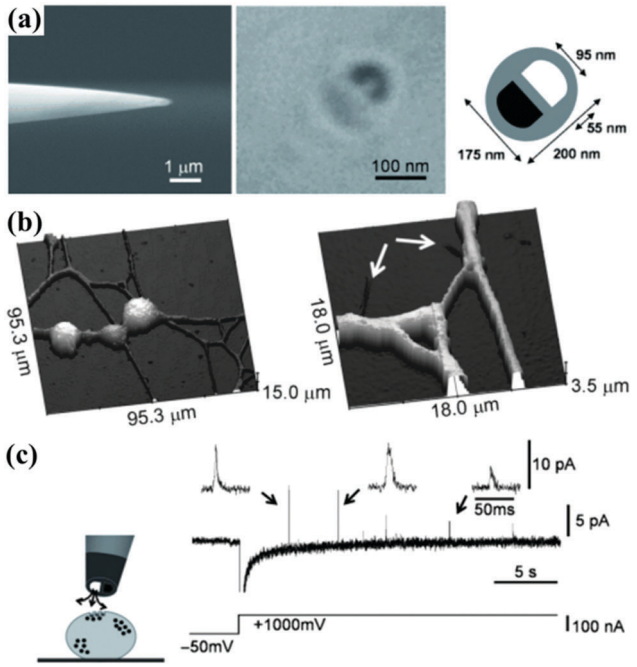

Fig. 18 (a) FE-SEM images of the side (left) and top (middle) view of the DBCNP. The specific size of the tip end of DBCNP is shown on the right. (b) Topographic images of differentiated PC12 cells using DBCNP. The arrows indicate the dendritic structures. (c) Schematic of the delivery of K^+ through DBCNP (left) to the cell. The current was observed by holding the DBCNP potential at 650 mV *vs.* Ag/AgCl (right). The spikes indicate that the neurotransmitter was captured by the DBCNP. Adapted with permission from ref. 78. Copyright 2011 Wiley-VCH Verlag GmbH & Co. KGaA, Weinheim.

and immobilized enzyme spots (*e.g.*, glucose oxidase (GOD) and horseradish peroxidase (HRP)) with a submicrometer resolution.[79] At the GOD spot, the distinct topographical features, which were described as "caves", were observed from both the SICM and SECM images at a close distance (~100 nm).

5. Future possibilities and prospects

What we call "imaging" depends highly on the resolution region. It is only for optical microscopic imaging in the roughly μm regime where we can actually "see" the enlarged image. For imaging in the nm region, either by electron or scanning probe microscopy, what is represented is usually an arbitrary color scale selected by the viewer, and thus subject to considerable manipulation.

Electrochemical imaging at the nm scale is an interesting new alternative. Unlike optical or electron-beam methods, SECM is not limited by diffraction and it does not require high energy or intense irradiation. Thus, the detection of single nm entities using SECM is not limited to specific fluorescent or Raman active molecules, and can be used with a wide range of insulating and conducting nm entities. SECM also differs from traditional scanning probe techniques such as tunneling and atomic force microscopy, in that the tip never contacts the surface. It is also carried out at ambient pressures and in liquids, a special advantage for biological samples. The possibility of improving resolution to the single molecule, atom, or clusters of atoms is encouraged by recent experiments, *e.g.* in ref. 80, where single Pt atoms were electrodeposited and then characterized electrochemically. Substantial additional studies are needed, however, to determine the scope of such analyses, which depend on electrocatalytic amplification.

Author contributions

All authors contributed equally to the manuscript.

Conflicts of interest

There are no conflicts to declare.

Acknowledgements

The support of the National Science Foundation to C.G.Z. (CHE-1757127), and the AFOSR MURI (FA9550-14-1-0003) and the Welch Foundation (F-0021) to A. J. B. are gratefully acknowledged.

References

1 A. J. Bard, F. R. F. Fan, J. Kwak and O. Lev, *Anal. Chem.*, 1989, **61**, 132.
2 *Scanning Electrochemical Microscopy*, ed. A. J. Bard and M. V. Mirkin, Taylor and Francis, Florida, 2nd edn, 2012.
3 J. Kim, J. E. Dick and A. J. Bard, *Acc. Chem. Res.*, 2016, **49**, 2587.
4 C. G. Zoski, *Current Opinion in Electrochemistry*, 2017, **1**, 46.
5 S. Amemiya, in *Nanoelectrochemistry*, ed. M. V. Mirkin and S. Amemiya, Taylor and Francis, New York, 2015, pp. 621–653.
6 S. Amemiya, in *Electroanalytical Chemistry: A Series of Advances*, ed. A. J. Bard, C. G. Zoski, Taylor and Francis, New York, 2015, pp. 1–72.
7 A. J. Bard, G. Denuault, C. Lee, D. Mandler and D. O. Wipf, *Acc. Chem. Res.*, 1990, **23**, 357.
8 C. Lee, J. Kwak and A. J. Bard, *Proc. Natl. Acad. Sci. U. S. A.*, 1990, **87**, 1740.
9 A. J. Bard, F.-R. F. Fan, D. T. Pierce, P. R. Unwin, D. O. Wipf and F. Zhou, *Science*, 1991, **254**, 68.
10 A. J. Bard, F.-R. F. Fan and M. V. Mirkin, in *Electroanalytical Chemistry*, ed. A. J. Bard, Marcel Dekker, New York, 1993, vol. 18, p. 243.
11 S. Amemiya, A. J. Bard, F.-R. F. Fan, M. V. Mirkin and P. R. Unwin, in *Annual Review of Analytical Chemistry*, ed. E. S. Yeung and R. N. Zare, Annual Reviews, CA, 2008, p. 95.
12 F.-R. F. Fan, J. Fernandez, B. Liu and J. Mauzeroll, in *Handbook of Electrochemistry*, ed. C. G. Zoski, Elsevier, Amsterdam, the Netherlands, 2007, Ch. 12, p. 471.
13 C. G. Zoski, in *Encyclopedia of Analytical Chemistry*, ed. R. A. Meyers, John Wiley & Sons, Ltd, Chichester, UK, 2011, vol. S1–S3, p. 1161.
14 C. G. Zoski, *J. Electrochem. Soc.*, 2016, **163**, H3088–H3100.
15 J. Rodrigueq-Lopez, C. G. Zoski and A. J. Bard, in *Scanning Electrochemical Microscopy*, ed. A. J. Bard and M. V. Mirkin, Taylor and Francis, New York, 2nd edn, 2012, ch. 16, p. 525.
16 D. Polcari, P. Dauphin-Ducharme and J. Mauzeroll, *Chem. Rev.*, 2016, **116**, 13234.
17 R. C. Engstrom and C. M. Pharr, *Anal. Chem.*, 1989, **61**, 1099A.
18 J. Kwak and A. J. Bard, *Anal. Chem.*, 1989, **61**, 1221.
19 J. Kwak and A. J. Bard, *Anal. Chem.*, 1989, **61**, 1794.
20 C. G. Zoski, J. C. Aguilar and A. J. Bard, *Anal. Chem.*, 2003, **75**, 2959.
21 Y. Saito, *Rev. Polarogr.*, 1968, **15**, 177.
22 C. G. Zoski and M. V. Mirkin, *Anal. Chem.*, 2002, **74**, 1986.
23 C. G. Zoski, B. Liu and A. J. Bard, *Anal. Chem.*, 2004, **76**, 3646.
24 F. M. Zhou, P. R. Unwin and A. J. Bard, *J. Phys. Chem.*, 1992, **96**, 4917.
25 K. C. Leonard and A. J. Bard, *J. Am. Chem. Soc.*, 2013, **135**, 15890.

26 R. C. Engstrom, M. Weber, D. J. Wunder, R. Burgess and S. Winquist, *Anal. Chem.*, 1986, **58**, 844.
27 R. C. Engstrom, T. Meaney, R. Topel and R. M. Wightman, *Anal. Chem.*, 1987, **59**, 2005.
28 R. C. Engstrom, R. M. Wightman and E. W. Kristensen, *Anal. Chem.*, 1988, **60**, 652.
29 C. G. Zoski, *Electroanalysis*, 2002, **14**, 1041.
30 P. Sun and M. V. Mirkin, *Anal. Chem.*, 2006, **78**, 6526.
31 B. Zhang, J. Galusha, P. G. Shiozawa, G. Wang, A. J. Bergren, R. M. Jones, R. J. White, E. N. Ervin, C. C. Cauley and H. S. White, *Anal. Chem.*, 2007, **79**, 4778.
32 *Ultramicroelectrodes, in Handbook of Electrochemistry*, ed. C. G. Zoski, Elsevier, Amsterdam, 2007, p. 155.
33 F.-R. F. Fan and C. Demaille, in *Scanning Electrochemical Microscopy*, ed. A. J. Bard and M. V. Mirkin, Taylor and Francis, New York, 2nd edn, 2012, p. 25.
34 M. V. Mirkin, in *Nanoelectrochemistry*, ed. M. V. Mirkin and S. Amemiya, Taylor and Francis, New York, 2015, ch. 15, p. 539.
35 N. Nioradze, R. Chen, J. Kim, M. Shen, P. Santhosh and S. Amemiya, *Anal. Chem.*, 2013, **85**, 6198.
36 J. Kim, C. Renault, N. Arroyo-Currás, N. Nioradze, K. C. Leonard and A. J. Bard, *Anal. Chem.*, 2016, **88**, 10284.
37 J. Kim, C. Renault, N. Arroyo-Currás, N. Nioradze, K. C. Leonard and A. J. Bard, *J. Am. Chem. Soc.*, 2016, **138**, 8560.
38 J. Chang, K. C. Leonard, S. K. Cho and A. J. Bard, *Anal. Chem.*, 2012, **84**, 5159.
39 W. Nogala, J. Velmurugan and M. V. Mirkin, *Anal. Chem.*, 2012, **84**, 5192.
40 T. Sun, P.-Y. Blanchard and M. V. Mirkin, *Anal. Chem.*, 2015, **87**, 4092.
41 M. Shen, N. Arroyo-Curras and A. J. Bard, *Anal. Chem.*, 2011, **83**, 9082.
42 J. Kim, B.-K. Kim, S. K. Cho and A. J. Bard, *J. Am. Chem. Soc.*, 2014, **136**, 8173.
43 C. M. Hill, J. Kim and A. J. Bard, *J. Am. Chem. Soc.*, 2015, **137**, 11321.
44 N. Nioradze, R. Chen, N. Kurapati, A. Khcataeva-Domanov, S. Mabic and S. Amemiya, *Anal. Chem.*, 2015, **87**, 4836.
45 J. Kim, M. Shen, N. Nioradze and S. Amemiya, *Anal. Chem.*, 2012, **84**, 3489.
46 C. Amatore and E. Maisonhaute, *Anal. Chem.*, 2005, **77**, 303a.
47 F. M. Zhou and A. J. Bard, *J. Am. Chem. Soc.*, 1994, **116**, 393.
48 S. P. Bi, B. Liu, F. R. F. Fan and A. J. Bard, *J. Am. Chem. Soc.*, 2005, **127**, 3690.
49 F. H. Cao, J. Kim and A. J. Bard, *J. Am. Chem. Soc.*, 2014, **136**, 18163.
50 J. H. Chang and A. J. Bard, *J. Am. Chem. Soc.*, 2014, **136**, 311.
51 M. Zhou, Y. Yu, K. K. Hu and M. V. Mirkin, *J. Am. Chem. Soc.*, 2015, **137**, 6517.
52 T. Kai, M. Zhou, Z. Duan, G. A. Henkelman and A. J. Bard, *J. Am. Chem. Soc.*, 2017, **139**, 18552.
53 M. V. Mirkin and A. J. Bard, *Anal. Chem.*, 1992, **64**, 2293.
54 M. Shen and A. J. Bard, *J. Am. Chem. Soc.*, 2011, **133**, 15737.
55 R. Chen, R. J. Balla, Z. T. Li, H. T. Liu and S. Amemiya, *Anal. Chem.*, 2016, **88**, 8323.
56 S. Y. Tan, J. Zhang, A. M. Bond, J. V. Macpherson and P. R. Unwin, *Anal. Chem.*, 2017, **89**, 7273.
57 S. Y. Tan, J. Zhang, A. M. Bond, J. V. Macpherson and P. R. Unwin, *Anal. Chem.*, 2016, **88**, 3272.
58 W. Ma, K. K. Hu, Q. J. Chen, M. Zhou, M. V. Mirkin and A. J. Bard, *Nano Lett.*, 2017, **17**, 4354.
59 T. Sun, Y. Yu, B. J. Zacher and M. V. Mirkin, *Angew. Chem., Int. Ed.*, 2014, **53**, 14120.
60 P. Y. Blanchard, T. Sun, Y. Yu, Z. Y. Wei, H. Matsui and M. V. Mirkin, *Langmuir*, 2016, **32**, 2500.
61 M. V. Mirkin, T. Sun, Y. Yu and M. Zhou, *Acc. Chem. Res.*, 2016, **49**, 2328.
62 P. Sun, F. O. Laforge, T. P. Abeyweera, S. A. Rotenberg, J. Carpino and M. V. Mirkin, *Proc. Natl. Acad. Sci. U. S. A.*, 2008, **105**, 443.
63 Y. Takahashi, A. I. Shevchuk, P. Novak, B. Babakinejad, J. Macpherson, P. R. Unwin, H. Shiku, J. Gorelik, D. Klenerman, Y. E. Korchev and T. Matsue, *Proc. Natl. Acad. Sci. U. S. A.*, 2012, **109**, 11540.
64 Y. Takahashi, A. Kumatani, H. Shiku and T. Matsue, *Anal. Chem.*, 2017, **89**, 342.
65 F.-R. F. Fan and A. J. Bard, *Proc. Natl. Acad. Sci. U. S. A.*, 1999, **96**, 14222.
66 S. Bergner, J. Wegener and F. M. Matysik, *Anal. Methods*, 2012, **4**, 623.
67 S. Bergner, J. Wegener and F.-M. Matysik, *Anal. Chem.*, 2011, **83**, 169.
68 Y. Wang, J. M. Noel, J. Velmurugan, W. Nogala, M. V. Mirkin, C. Lu, M. Guille Collignon, F. Lemaitre and C. Amatore, *Proc. Natl. Acad. Sci. U. S. A.*, 2012, **109**, 11534.
69 Y. Li, K. Hu, Y. Yu, S. A. Rotenberg, C. Amatore and M. V. Mirkin, *J. Am. Chem. Soc.*, 2017, **139**, 13055.
70 Y. Takahashi, T. Miyamoto, H. Shiku, R. Asano, T. Yasukawa, I. Kumagai and T. Matsue, *Anal. Chem.*, 2009, **81**, 2785.
71 K. Huang, A. Anne, M. A. Bahri and C. Demaille, *ACS Nano*, 2013, **7**, 4151.
72 L. Nault, C. Taofifenua, A. Anne, A. Chovin, C. Demaille, J. Besong-Ndika, D. Cardinale, N. Carette, T. Michon and J. Walter, *ACS Nano*, 2015, **9**, 4911.
73 J. V. Macpherson, C. E. Jones, A. L. Barker and P. R. Unwin, *Anal. Chem.*, 2002, **74**, 1841.
74 M. R. Gullo, P. L. T. M. Frederix, T. Akiyama, A. Engel, N. F. deRooij and U. Staufer, *Anal. Chem.*, 2006, **78**, 5436.
75 A. J. Wain, A. J. Pollard and C. Richter, *Anal. Chem.*, 2014, **86**, 5143.
76 D. J. Comstock, J. W. Elam, M. J. Pellin and M. C. Hersam, *Anal. Chem.*, 2010, **82**, 1270.
77 C. A. Morris, C. C. Chen and L. A. Baker, *Analyst*, 2012, **137**, 2933.
78 Y. Takahashi, A. I. Shevchuk, P. Novak, Y. J. Zhang, N. Ebejer, J. V. Macpherson, P. R. Unwin, A. J. Pollard, D. Roy, C. A. Clifford, H. Shiku, T. Matsue, D. Klenerman and Y. E. Korchev, *Angew. Chem., Int. Ed.*, 2011, **50**, 9638.
79 Y. Takahashi, A. I. Shevchuk, P. Novak, Y. Murakami, H. Shiku, Y. E. Korchev and T. Matsue, *J. Am. Chem. Soc.*, 2010, **132**, 10118.
80 M. Zhou, J. E. Dick and A. J. Bard, *J. Am. Chem. Soc.*, 2017, **139**, 17677.